**Utrecht University**

# An analysis of the data from the HiSPARC-detectors

**Bachelor thesis by Carleen van Hengel**
17 june 2015

Faculty of Sciences
Department of Physics & Astronomy

**Institute for Subatomic physics**
Supervisors:
André Mischke
Alessandro Gerlli

**Abstract**

Cosmic rays are extra-terrestrial particles that undergo interactions when they enter the atmosphere. They cause a cascade of new particles such as muons, electrons and photons. These particles reach the ground and pass through a scintillator in which they excite an electron of a fluorescent atom, these new photons will then be converted into a electronic signal by a photon multiplier and information of the pulse will be stored if in both plates of the detector within the coincidence time a pulse is measured.
With this data can be determined if the detector works correctly. At a certain energy the pulse height will be thus high that the pulse integral is saturated, this occurs from 1800 ADC. The arrival time difference distribution is a Gaussian with the mean the consistent difference in arrival time of the pulse between the two plates. Both the mean and the sigma of the Gaussian are stable in time. The ratio of the frequency of a certain amount of muons between the two plates is one up till ten muons in the plate per event. After that is shows a trend downward. The pulseheight distribution for a certain amount of muons consists of a Gaussian with a Landau. The peaks are shifted to higher energy for higher amount of muons, however the peak of the distribution with two muons in a plate is not two times the peak position of one muon in a plate. Temperature influences the average muon rate positive, whereas humidity influences it negative. There is no correlation between pressure and the average amount of muons per event. The average amount of muons per hour shows a minimum around midday and two maxima three hours before and after midnight. When compensated for temperature and humidity difference there are on average more muons reaching the earth in winter.

# Contents

# 1 Introduction

In 1785 Coulomb discovered that electroscopes discharge spontaneously in air, even when no X-ray tubes or radioactive materials where near it [1]. In 1903 if was found that the electroscopes would discharge more slowly if they were shielded by metal [2, 3]. Meaning that the radiation was not spontaneously generated inside the electroscope. Kurz concluded in 1909 that there were three possible origins of the radiation. It was either caused by the atmosphere, the crust of the earth of it was extra-terrestrial. Different experiments were carried out with contradicting results, some stated the radiation to be extra-terrestrial other that it came from the earth's crust. In 1911 and 1912 Hess made balloon flights up to 5 kilometres [5]. He found a decrease in the intensity of the radiation in the first few hundred meters above the ground, but above that the intensity increased, which resulted in the conclusion that the radiation is extra-terrestrial [6]. Millikan and Cameron submerged electroscopes in lakes at different altitudes and also concluded that the origin of the radiation was extra-terrestrial [7]. Millikan called the radiation cosmic rays. Up till that point only gamma rays were considered as part of cosmic rays. In 1923 Compton established that the rays intensities depended on latitude, due to the earth's magnetic field, and that cosmic rays were mainly made up of charged particles [8].
Nowadays, we are interested in what kind of particles cosmic rays are made up of, with what energy they approach the earth and where they come from. Therefore, detectors are build, such as the HiSPARC (High School Project on Astrophysics Research with Cosmics) detectors. Also it is needed that the detector works properly and to know what influences the detector.
In the first section the sources and properties of cosmic rays will be described along with what happens with the cosmic ray particles when they enter the atmosphere. The section on HiSPARC will explain the HiSPARC detectors and the data acquisition from these detectors more detailed. In the section after that several data analysis will be applied to the acquired data. Also the influence of weather conditions will be researched as well as the change in particle flux between day and night and the particle flux difference between summer and winter. The final section will conclude on the results and provide an outlook for future research.

# 2 Cosmic rays

## 2.1 Properties

The majority of the initial cosmic ray particles are protons (84 % ) and alpha particles (12 % ). The remainder is nearly all heavier nuclei and electrons make up less than 1 % [14].
The chemical abundancy of the cosmic rays is similar to the abundancy of elements of the solar system, see figure 1. However, due to interaction with the interstellar medium (ISM) nuclei can be split, this is called spalliation. This results in a higher abundance for sub-iron elements as Sc, Ti, V, Cv and Hn. The same goes for the more abundant nuclei of Li, Be and B due to the spalliation of elements C and O.

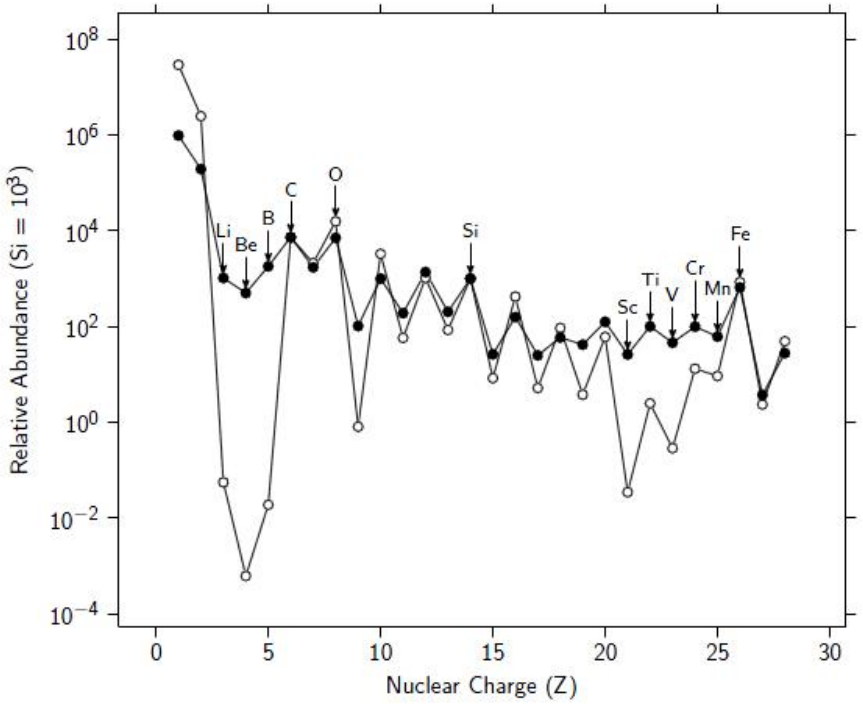


Figure 1: Chemical abundancy in the solar system. Open circles is average for the solar system. Closed circles is measured during a solar minimum. From Thesis Dr. Fokkema [9], where it is redrawn from [10, 11, 12, 13].

Antiparticles are rare in cosmic rays, the ones that are in it, are there due to interaction with the ISM [15, 16]. proton-proton collisions result in antinucleons and positrons are generated along with an electron by pair creation.
Low energy particles of the cosmic rays are deflected by the magnetic fields of both the earth and the Sun. If the energies of the particles are even lower, they can get trapped

in the Van Allen radiation belts around the Earth. These particles enter the atmosphere at the poles, producing the aurora.
The particles that enter our atmosphere are mainly protons and electrons from the solar wind. These particles have energies in the order of MeV. The interplanery magnetic field depends on the solar cycle and a high solar activity results in a stronger field and thereby fewer cosmic rays.
The energy spectrum of the cosmic rays follows a power law for energies above 10 GeV. $E-\gamma$), with spectral index $\gamma \sim 3$, as can be seen in figure 2.

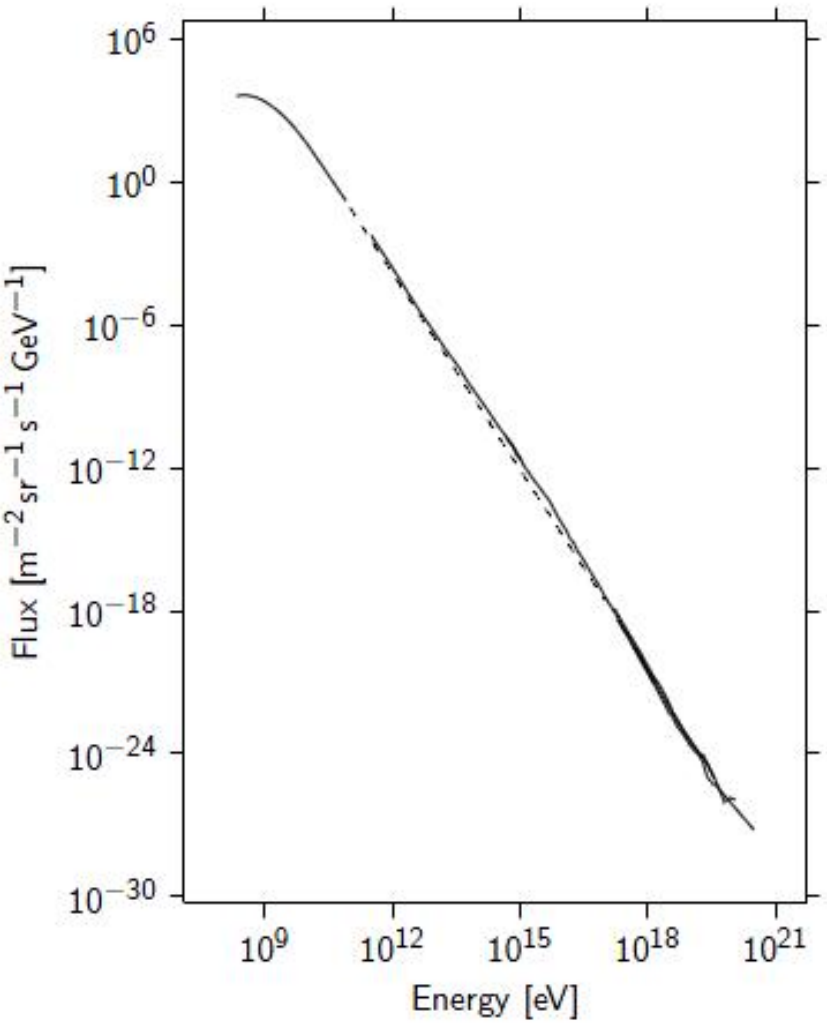


Figure 2: Flux versus the energy of the cosmic ray particle [20].

Around E $\approx$ 4 PeV the spectrum becomes steeper and the spectral index changes from 2.7 to 3.1 [17]. This is called the knee. Cosmic ray particles are mainly produced in our

galaxy and are contained in it by the galactic magnetic field. Above a certain energy cosmic rays can escape and therefore less particles with this energy will reach the earth. The energy level at the knee could also be the maximum energy at which particles of the cosmic rays can be accelerated by sources in our galaxy [18]. Heavy nuclei can be accelerated faster than protons without being able to leak away from our galaxy. At the knee the composition of cosmic rays also changes from protons to iron nuclei [19].
There are cosmic rays with energies significantly above the knee, these must originate from sources outside our galaxy. At this high energy the spectrum becomes less steep. This change in slope is called the ankle. According to Greisen, Zatsepin and Kuzmin at ultra high energies the cosmic rays will interact with the cosmic microwave background (CMB), resulting in a limit for the energy of the cosmic ray particles, the GZK-limit. The cosmic ray particle interacts with a CMB photon creating a pion, this results in energy loss for the cosmic ray particle, and as long as the energy of the particle is above the pion threshold it will keep interacting with the CMB resulting in more energy loss. This gives a pile-up of cosmic rays with an energy just below the GZK-limit, which could explain the smaller slope around the ankle. If a source that produces cosmic rays with energies above the GZK-limit it should be within 50 Mpc [1] in order to be detected on earth, otherwise the energy of the particle will drop below the limit before it reaches the earth.
Due to deflection of cosmic ray particles by the galactic magnetic field the direction of arrival is not correlated with the direction of the source for cosmic ray particles with energies lower than 100 TeV. The distribution of cosmic rays is then nearly isotropic. When the energy is higher than $10^{19}$ eV the direction of arrival is related to the direction of the source.

### 2.2 Sources for cosmic rays

There are different acceleration mechanisms to give the cosmic ray particle its energy. The direct acceleration with rotating magnetic fields require large sixed accelerators or massive magnetic fields and only few sources for cosmic rays, such as sun spots, pulsars, interstellar clouds and shock wave fronts, remain.
One of these acceleration mechanisms is fermi acceleration [21]. This is schematically shown in figure 3a. The interstellar medium is filled with turbulent magnetic fields, and in interstellar clouds these are the strongest. If a particle moves in the opposite direction of such a cloud then in the reference frame of the cloud the particle is reflected elastically. This reflection is due to the magnetic field. However, in the lab frame the particle gains velocity, thus kinetic energy. If its the other way around, the cloud and the particle move in the same direction, it loses energy. However, the cloud usually moves faster than the particle and therefore collisions with opposite directions are more likely to occur.
Shown in figure 3b is another acceleration mechanism is shock acceleration. During supernovas a shock wave, driving interstellar matter outward, is generated. This shock wave travels faster than the stellar matter of the supernova. Due to this speed difference there are only particles that travel in opposite direction of the shock wave. In the frame that

[1] Parsec (pc) is the astronomical unit of length, 50 Mpc corresponds to $1,5 \cdot 10^{21}$ km

moves with the shock front gas before the shock front has a different velocity than gas that has already passed the shock front. The particle is reflected after it passes the shock front and passes the shock front once more, having gained velocity. The particle can be reflected by the magnetic field on the other side of the shock wave as well, and pass the shock front again. This can occur countless times and therefore result in a large energy gain.

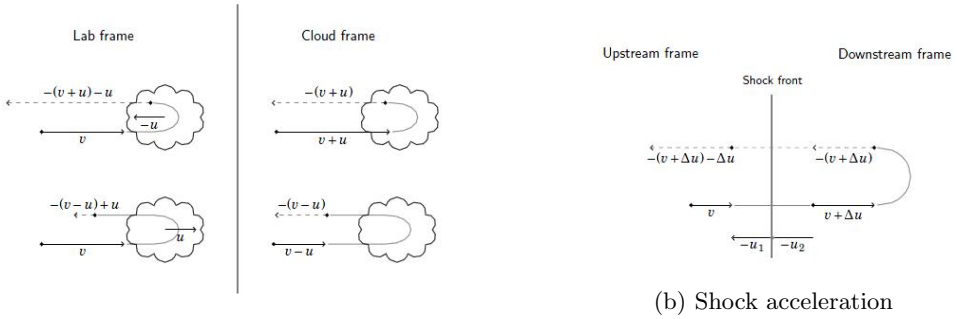


(a) Fermi acceleration

(b) Shock acceleration

Figure 3: Scematic representations of the acceleration mechanisms [9].

## 2.3 Cosmic ray showers

When a cosmic ray particle enters the atmosphere it interacts with particles that make up the atmosphere. Photons can ionize atoms due to interaction with electrons, as a result the photons lose energy, this is called Compton scattering. Photons can undergo pair production, creating particle-antiparticle pairs. Charged particles can be excited or ionize atoms by transferring energy to electrons, this process is called ionization energy loss. Bremsstrahlung is when charged particles radiate photons due to interaction with the electric field of a nuclei. The charged particles can also radiate photons due to interaction with the earth magnetic field; this is called synchrotron radiation.
At an height of about 20 to 15 km the first interaction occurs. It produces secondary particles, whom will interact as well and generate tertiary particles and so on. Until the energy of a particle drops below the energy required to create new particles. All the particles created are called a cascade or shower, schematically this is shown in figure 4. The particles that reach the ground can have a footprint up to several square kilometres.

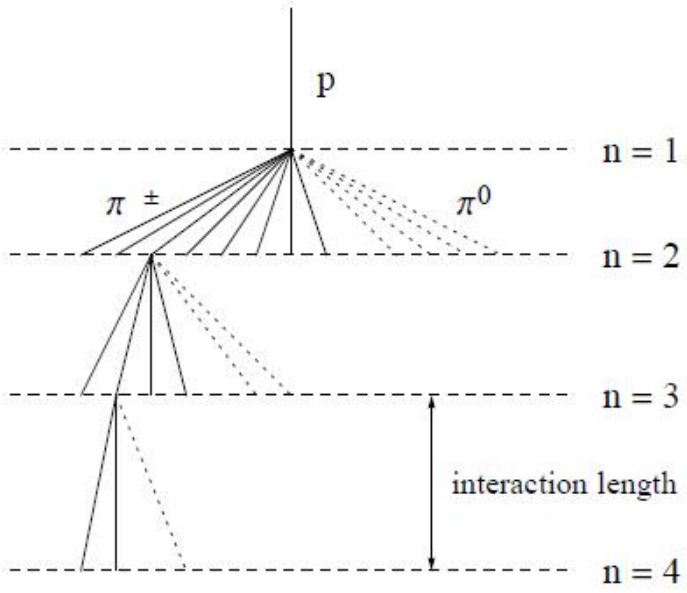


Figure 4: Scematic representation of a shower [22].

Electromagnetic cascades consist of electrons and photons, they are either part of the cosmic rays or secondary particles from interaction of cosmic ray particles that are nuclei. At high energy pair production and Bremsstrahlung are the main sources of electrons and photons

$e \to e + \gamma$ and $\gamma^* \to e^- + e^+$.

The Heitler model describes this process [23]. After an interaction length $\lambda$ the particle interacts and creates two particles with each half the parent energy. Therefore, after n interactions there will be $2^n$ particles with each $E = E_0/2^n$, where $E_0$ is the energy of the primary particle. This model works until the energy drops below the energy needed create new particles, but the absorption is not described.
Hadronic cascades consists of cascades generated by a cosmic ray proton or nuclei. This results mainly in the creation of pions and kaons. The pions can decay in muons, electrons, neutrinos and photons

$\pi^+ \to \mu^+ + v_\mu$, $\pi^- \to \mu^- + \overline{v_\mu}$ and $\pi^0 \to \gamma + \gamma$ .

Kaons mainly decay into pions, muons, electrons and neutrinos. The muons decay in electrons and positrons.

$\mu^+ \to e^+ + v_e$ and $\mu^- \to e^- + \overline{v_e}$.

Due to the constant generation of electrons and photons the majority of the energy of the primary particle is transferred into electromagnetic cascade.

Atmospheric depth is the amount of matter between a certain height $h$ and the atmosphere above it

$$X = \int_h^\infty \rho(h')dh'. \tag{1}$$

If the atmosphere were to be an ideal gas with a constant temperature and in hydrostatic equilibrium equation 1 would become $X = X_0 \exp(-h/h_0)$, with $X_0$ the atmospheric depth at sea level and $h_0$ the scale height of the atmosphere [24]. This approximation is not correct for the atmosphere on Earth. However, the atmosphere can be divided into different layers with each a different approximation of equation 1.
Cosmic ray particles do not necessarily enter the atmosphere perpendicular to the surface of the earth, but with an inclination $\theta$. If the earth is approximated to be flat then $X' = X \cos(\theta)$. How much of the atmosphere is travelled through, $X'$, is called slant depth. If the inclination angle is smaller than 60°, considering the earth as a flat surface is a good approximation. For larger angles the approximation no longer holds and the curved surface of the earth needs to be taken into account.
The radiation length is the distance over which the energy of an high-energy electron is reduced by a factor $1/e$. For air this is 36.66 g/cm$^2$. The average distance in which a high-energy hadron undergoes interaction is called the interaction length. For air this is 90.0 g/cm$^2$. The total atmosphere has a depth of 11 interaction lengths and 28 radiation lengths.
For an accurate parameterization of the longitudinal development of the shower the Rossi and Greisen model can be used

$$N(t) \sim t^\alpha \exp(-\beta t) \ .$$

In this formula $t = x/X_0$, with $X_0$ the radiation length and $x$ the depth. $\alpha$ and $\beta$ are parameters for the creation and absorption of particles [14].
However the shower does not only progress in the z-direction, but it also expands in the x-y plane due to scattering and transverse momenta. As illustrated in figure 5, at sea level the shower core is mainly made up of photons and electrons. At distances further away from the shower core the number of muons is roughly the same of even larger than that of the number of electrons.

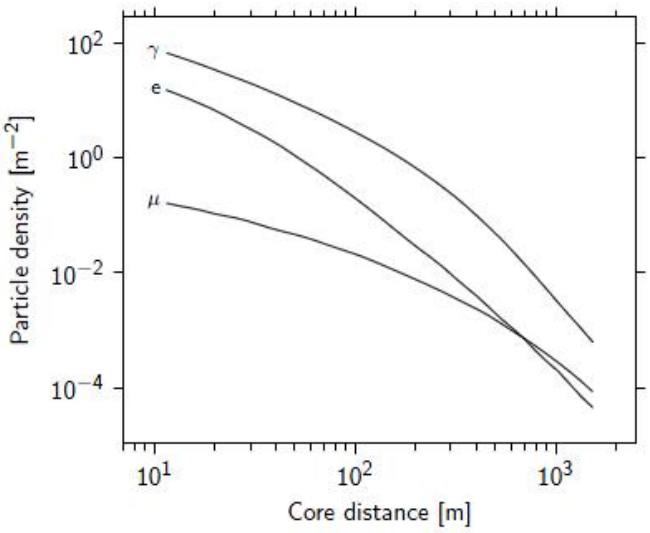


Figure 5: Density of particles versus the distance from the shower core [9].

This due to the fact that muons are created high in the atmosphere and have few interactions until they reach the ground. Therefore, their development in the lateral direction is similar to $\langle x \rangle \propto h$. Whilst electrons are created in the entire shower and undergo a random walk, this leads to a different profile in the x-y plane: $\langle x \rangle \propto \sqrt{h}$.
The lifetime of a muon is 2.2 $\mu$s, which is not long enough to reach the ground in a reference frame on the ground, but due to its high velocity the Lorenz factor is high enough in order for the muons to reach the ground, within 2.2 $\mu$s in their own reference frame. The decay length then becomes about 6.2 km and the flux of muons on ground level is 1 cm$^{-2}$/min [14]. If the primary particle has an energy of 100 TeV then at sea level only 10% of the charged particles are muons, the rest are $e^-$ and $e^+$.

# 3 HiSPARC

HiSPARC is a project that studies cosmic rays and allows high school students to get inside in cosmic ray research. High school students will build their own detector and this detector contributes to the array of detectors, which allows for air showers to be detected and analyzed. With the data from the HiSPARC website, where all data from all the stations is retrievable, high school students can also perform data analysis and with Excel they can plot the pulseheight distribution, in intervals of energy the amount of times a pulseheight is within each interval is counted, muon ratio, a histogram similar to the one for the pulseheight is made and for every corresponding number of muons the counts are divided by one another and difference in arrival time, the difference in arrival time is calculated and a histogram is made.

## 3.1 experimental setup

A scintillator is used to detect particles. The base of the scintillator is polyvinyltoluene, a plastic, this is doped with fluorescent particles, in this case fluor. The fluor particles are excited when particles pass through the scintillator. When the electron returns to its ground state photons are emitted. This decay has a time frame of 2.1 ns.
The scintillator is 1 m x 0.5 m. A light guide is glued to one of the shorter edges of the scintillator and has a triangular shape, in order to lead the photons to the photomultiplier (PMT), which is attached to the other end of the light guide. The scintillator and the light guide are wrapped in aluminium foil to prevent any light exiting. The entire plate, scintillator and light guide, is then wrapped in black plastic in order to prevent any light from coming in. Muons, photons and electrons that are detected by the detector will pass though all this material.

The photomultiplier attached to the light guide converts the photons from the scintillator to an electrical signal. The PMT is connected to an analogue to digital converter (ADC), that converts the electrical signal into a signal that can be processed by a computer. The PMT is made up of an cathode. A photon reaches the cathode and a electron is emitted due the photoelectric effect. Then the electron is drawn to the first dynode due to the positive potential over the dynode. When the electron hits the dynode more electrons are released and directed to the next dynode. Every electron frees new electrons, so over several dynodes an avalanche of electrons occurs. Because there are more electrons after every dynode is hit, consecutive dynodes have a higher voltage. After the last dynode the electrons reach the anode from where the current pulse goes to the ADC.
The PMTs operate at a certain voltage. If the voltage is too low, the signal will not be clear enough, if the voltage is too high, electrons will be freed from the dynodes at the smallest disturbance. Assuming the rate of particles is stable, then for equal time intervals we can measure the amount of particles when the PMT is connected to different voltages. If the PMT works properly, as can be seen in figure 6a then there is a plateau in the curve, a voltage range for which the counts are stable. The voltage on which the

PMT operates should be set on a voltage on the plateau. When a PMT is broken this plateau is not visible, as is shown in figure 6b.

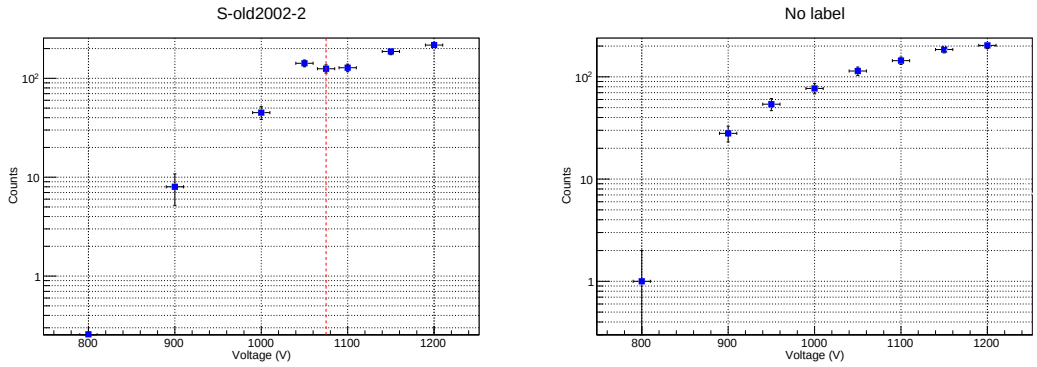


(a) Functioning PMT

(b) Broken PMT

Figure 6: For different voltages the amount of registered pulses is counted for five minutes. The voltage is set against the number of counts. In 6a the plateau is visible, whilst there is no plateau in 6b.

A detection station is made up of two or four plates. Every plate is stored in their own ski box and placed on the roof of the same building, as illustrated in figure 7b. The ski boxes are used to protect the plates from the weather conditions. In case of a station with two plates the boxes are placed at least five meters apart. In the middle a GPS, that determines the location of the station and is used to measure the date and time of an event. The setup is shown in figure 8. Most detectors are part of a cluster; a group of detectors positioned closely together, they are only a few hundred meters or kilometres apart. With a cluster the direction and energy of a shower can be determined.

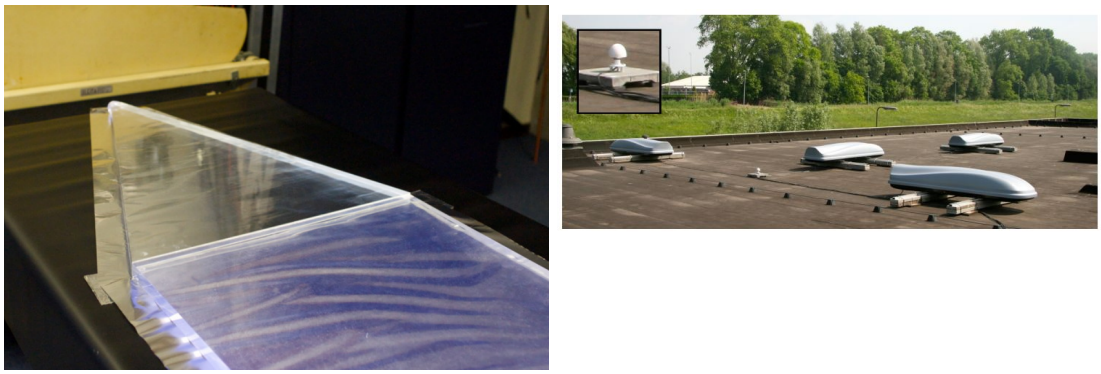

(a) Construction

(b) Roof setup

Figure 7: In fig 7a the scintillator with a light guider wrapped in aluminium attached to it is shown [26]. In fig 7b the setup of a detector consisting of four plates and a GPS is shown [9].

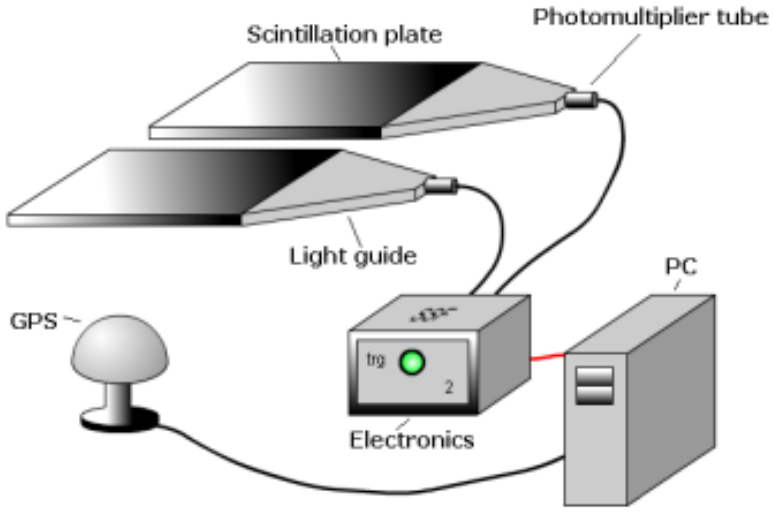


Figure 8: Schematic representation of the setup of a HiSPARC detector [25].

### 3.2 Data acquisition

In figure 9, the signal received from the PMT is shown. If this signal is below a certain threshold, usually -70 mV, a trigger is issued and the incoming data is stored in a buffer. If the other plate reaches the threshold as well, within the coincidence window of 1.5 $\mu s$, the data is stored. Data from $1\mu s$ until $3.5\mu s$ after the coincidence window is recorded. In this $6\mu s$ window no trigger for a new event is allowed. The output from the PMT connected to a trigger matrix that regulates this.
The date and time of an event is determined by the GPS attached to the setup. Other information such as pulseheight, the integral of the pulseheight, arrival time and amount of muons are stored for both plates.

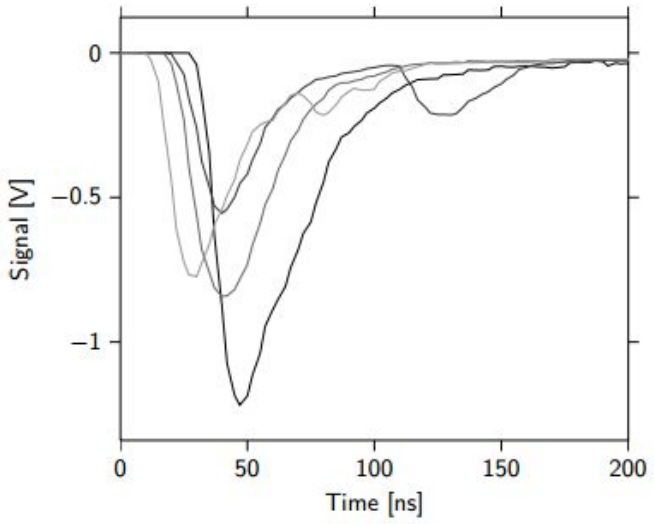


Figure 9: A typical signal of a PMT [9].

The pulseheight spectrum can be constructed by counting the amount of times a certain energy occurs. This spectrum is shown in figure 10. The spectrum consists of two shapes. One is an exponential decreasing function at low energies, this are the photons and electrons. The other shape is a convolution of Landau distributions. Every distribution represents a different amount of muons that passed through the plate.

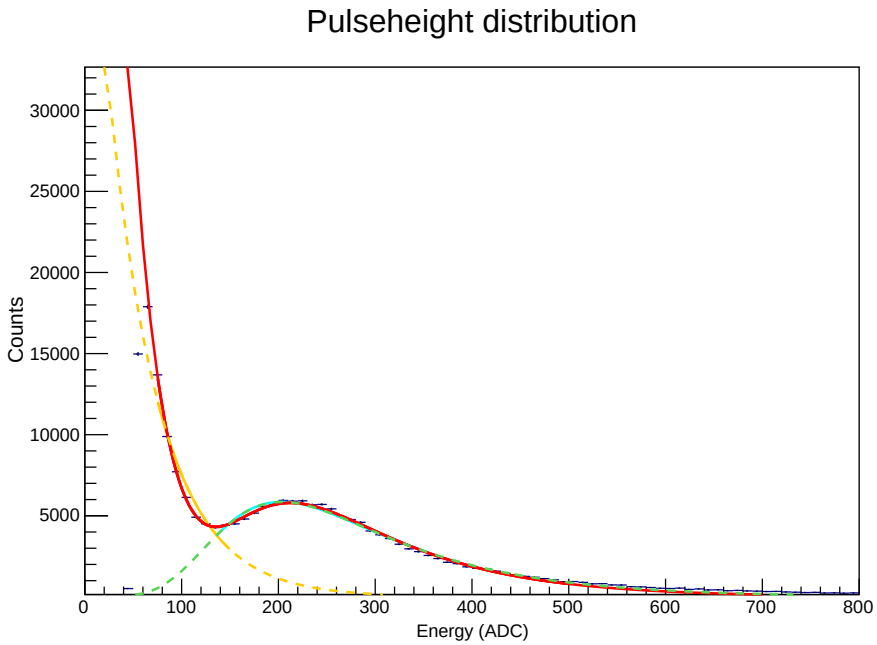


Figure 10: Histogram of the pulse height, with a fit of an exponential and Landau function, for one muon passing through the plate.

HiSPARC data from all of the detectors can be downloaded from the HiSPARC website in a csv-file [27]. This can then be converted into a ROOT-file, on screen representation can be seen in figure 11. A ROOT-file consists of a tree with different branches. In each of the branches a specific part of the data set, for instance pulseheight, is stored. Every event registered by the detector corresponds to a certain entry number. These different branches can then be used for the data analysis.

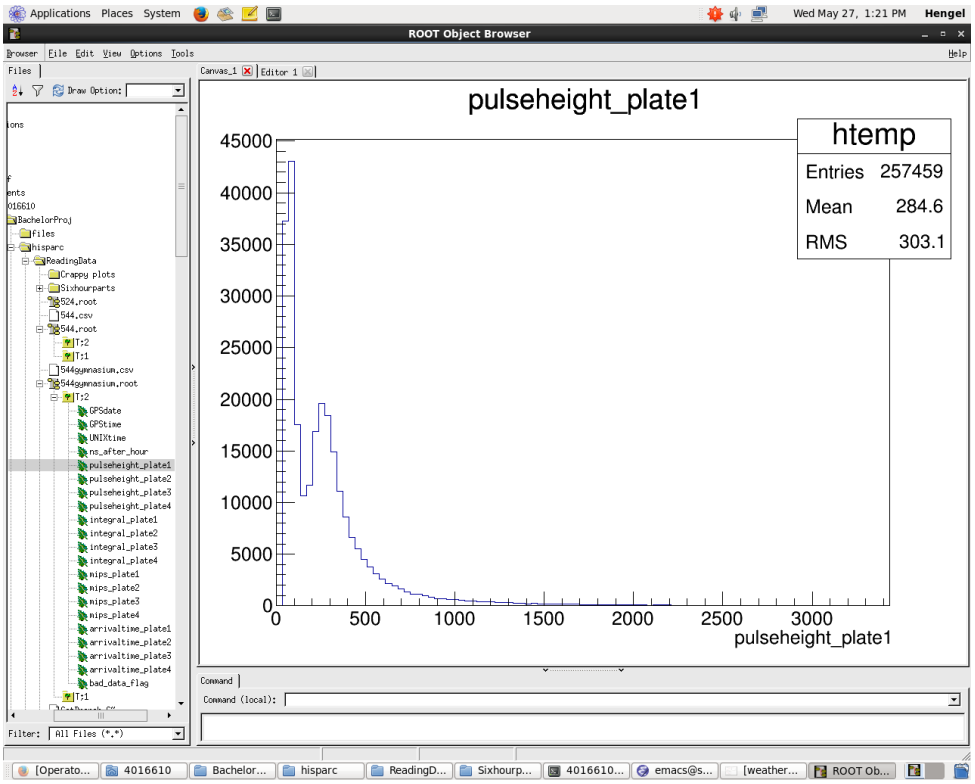


Figure 11: On screen representation of a ROOT-file, on the left side the tree with the branches can be seen.

# 4 Data analysis

## 4.1 Dataset

In this data analysis the detector stations of the Utrecht cluster will be considered (station number 1001 till 1010). The locations of these stations are displayed in figure 12. For analysis of station specific properties five working stations will be used. Specific properties are PMT saturation and difference in arrival time between the plates. For studied effects that should be consistent for all detectors station 1001 of Utrecht University is used.

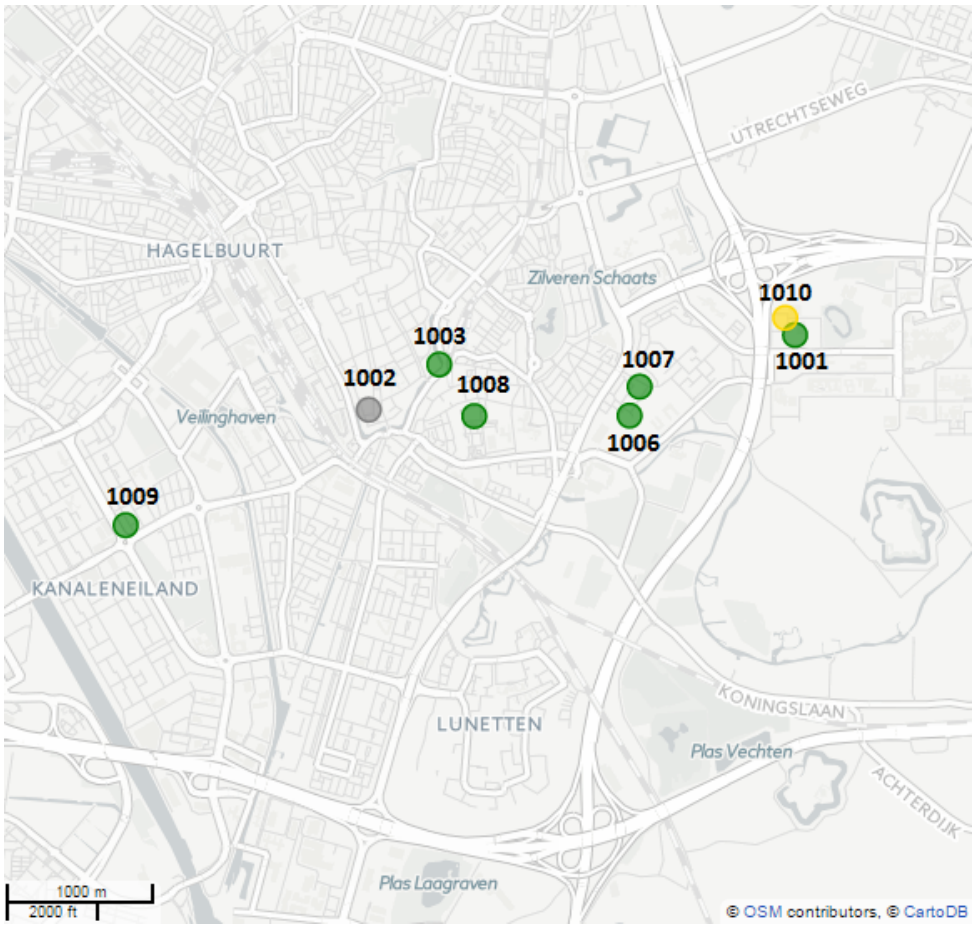


Figure 12: Stations in the Utrecht area, working stations are indicated by a green circle, stations that are no longer operational with a grey circle and stations with a problem are displayed as yellow circles [28].

## 4.2 Pulseheight versus pulse integral

Several aspects of the pulse of an event are stored, including pulseheight and the pulse integral. To see if a plate is working properly one can set the pulseheight against the

| Station number | 1001 | 1003 | 1006 | 1007 | 1008 |
|---|---|---|---|---|---|
| Plate 1 (ADC) | $2800 \pm 100$ | $2100 \pm 100$ | $2500 \pm 100$ | $2300 \pm 100$ | $2400 \pm 100$ |
| Plate 2 (ADC) | $2400 \pm 100$ | $2400 \pm 100$ | $1800 \pm 100$ | $2300 \pm 100$ | $2100 \pm 100$ |

Table 1: For all operational stations in the Utrecht area the value of the pulseheight for which the pulseheight versus the pulse integral ceases to be linear.

pulse integral, as shown in figure 13. For pulses with low energies the pulseheight and pulse integral will have a linear relation. As the height of the pulse gets higher the pulse gets narrower, resulting in a saturation of the pulse integral and the slope of the curve flattening. In table 1 the values where the relation ceases to be linear is shown. The flattening occurs at different energies but the range is 1800 till 2800 (ADC).

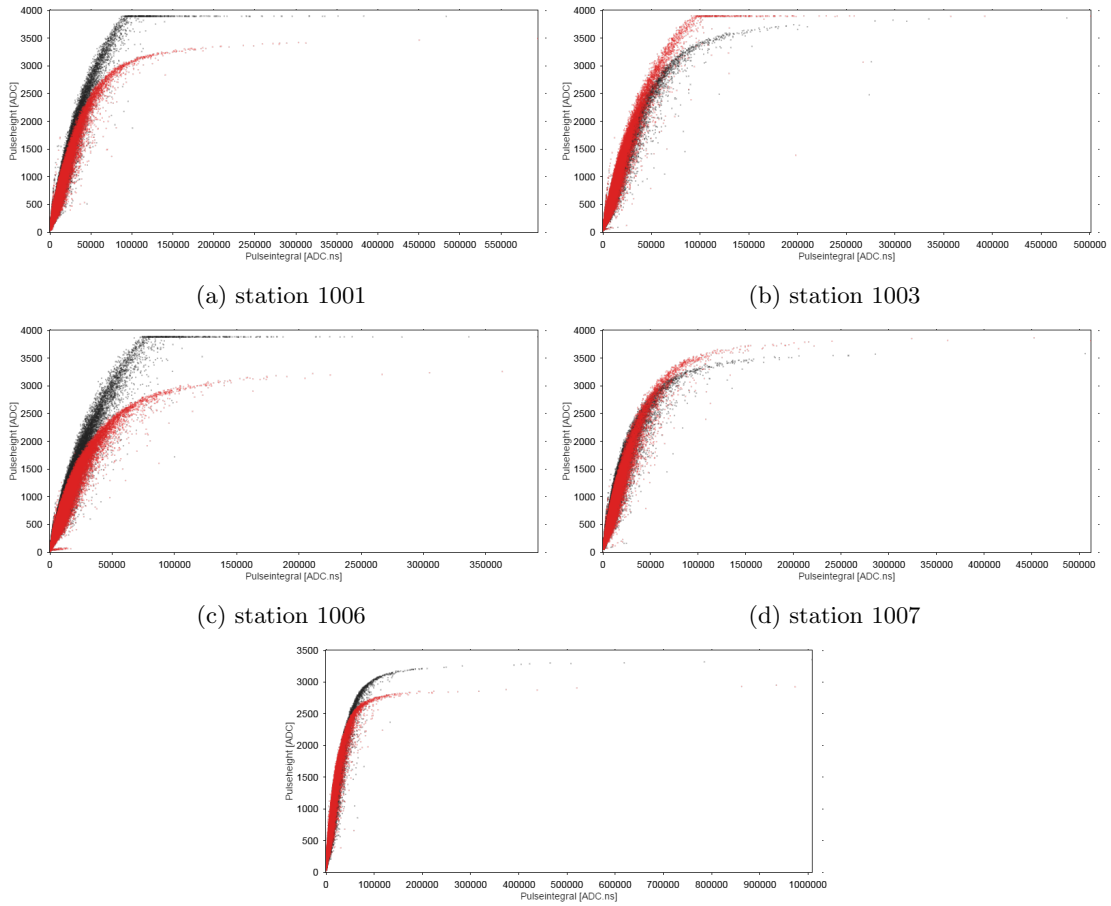


(a) station 1001

(b) station 1003

(c) station 1006

(d) station 1007

(e) station 1008

Figure 13: Pulseheight plotted against the pulse integral of both plates (plate 1 in black and plate 2 in red) for each of the operational stations in Utrecht.

### 4.3 Arrival time

In the data stored from the events is the arrival times of the pulses of the same event of both plates. The difference in arrival time between the two plates should averaged over time be zero. However, there will be a spread in arrival time, not all showers come in perpendicular to the plates, and the shower front has a thickness. Therefore, we would expect the distribution of the difference in arrival time between the two plates to have the shape of a Gaussian. When a detector does not work correctly this distribution will be distorted, as can be seen in figure 14. For the stations in the Utrecht area that function properly the distributions are Gaussians, this is shown in figure 15. The reduced $\chi^2$ is a measure for the goodness of the fit, the mean tells us the shift of the Gaussian and the sigma of the Gaussian shows us the resolution of the detector. These results are summarised for all stations in figure 16.

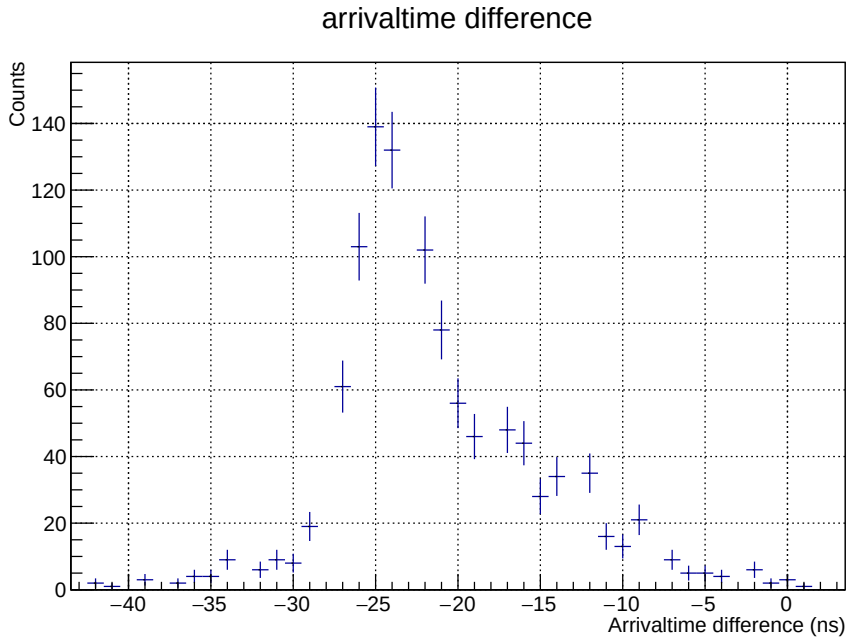


Figure 14: The difference in arrival time for station 1009, during the time it was not functioning properly. The shape of the distribution is not just one Gaussian and it is not centred around zero.

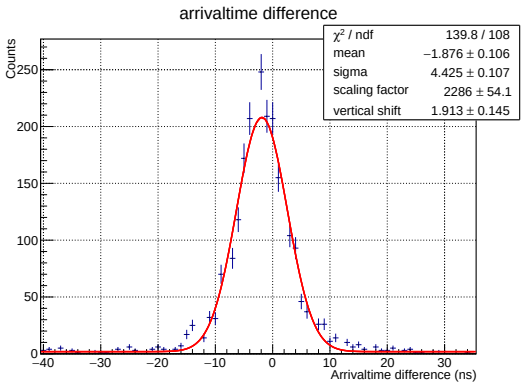


(a) station 1001

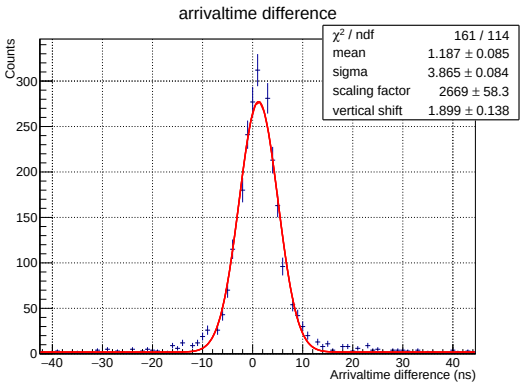


(b) station 1003

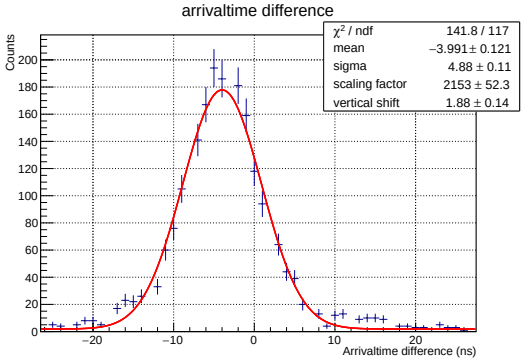


(c) station 1006

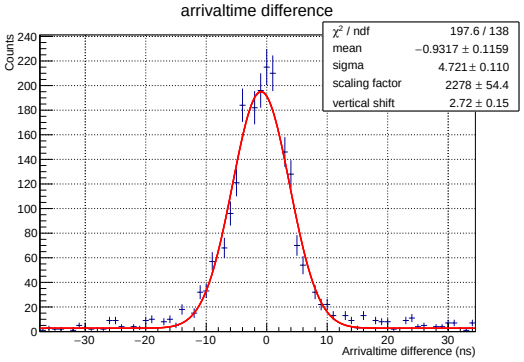


(d) station 1007

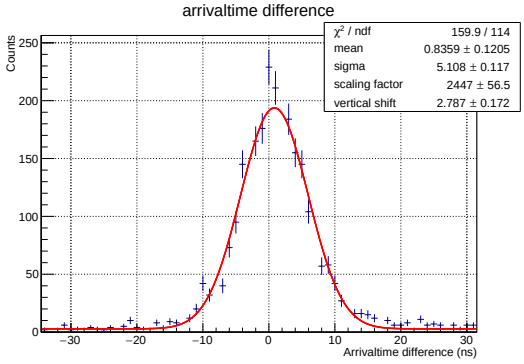


(e) station 1008

Figure 15: The difference in arrival time for station all operational stations in the Utrecht area. All fits (red curve) are Gaussians.

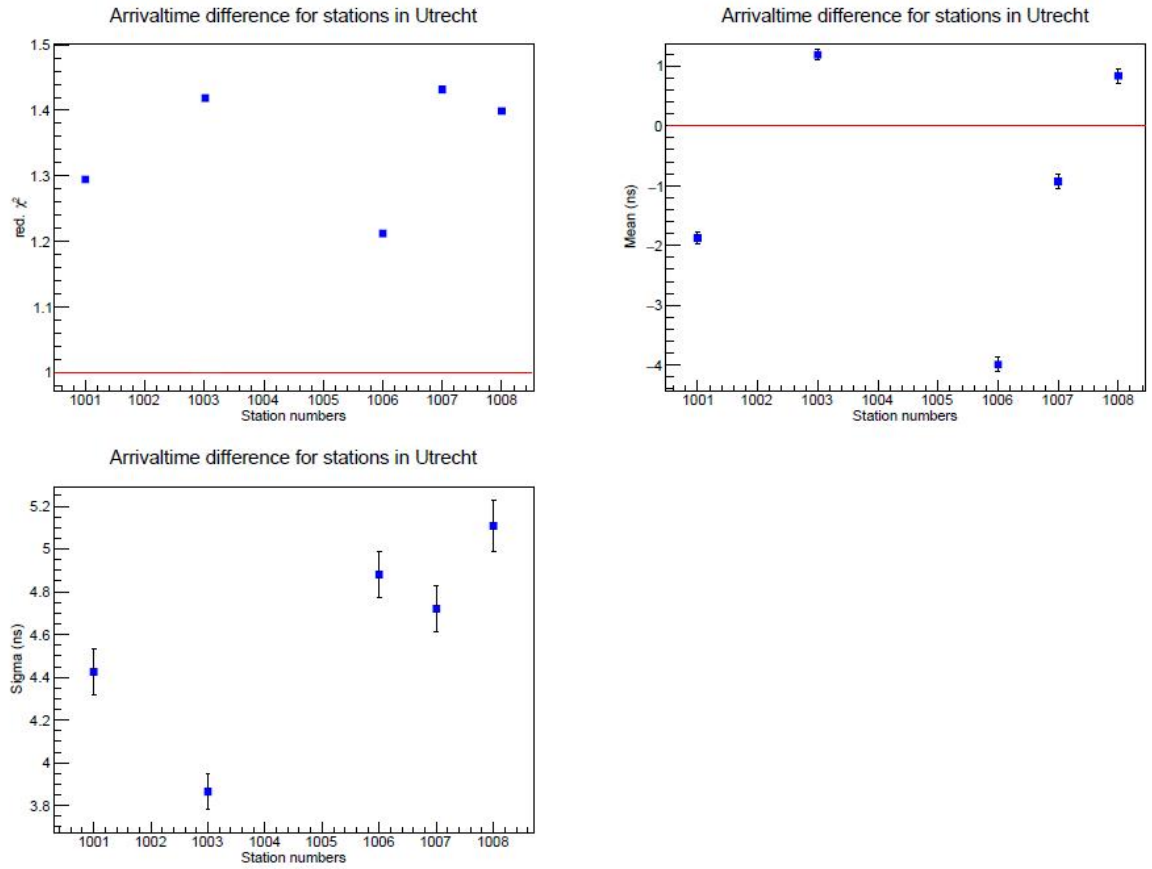


Figure 16: For all operational stations in the Utrecht area the reduced $\chi^2$, the mean and the sigma of the Gaussian fitted to the distribution of the difference in arrival time is shown.

In figure 17, the time evolution of the mean and the sigma of the fitted Gaussian are depicted for two detectors. For both detectors the same time period is taken. The figure illustrates that during the two weeks the means go up and the sigmas go down. However, the slopes are very small, less than 0.2%, and we can conclude that the mean and the sigma are stable in time.

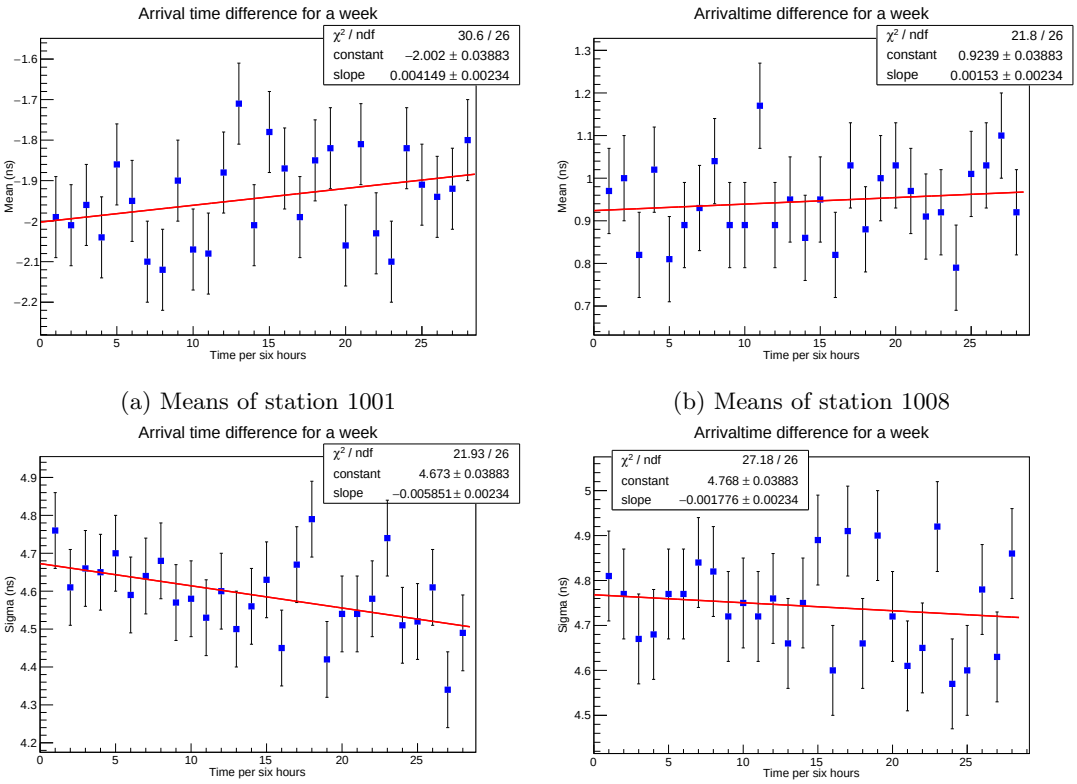


(a) Means of station 1001

(b) Means of station 1008

(c) Sigmas of station 1001

(d) Sigmas of station 1008

Figure 17: For stations 1001 and 1008 over the course of two weeks every six hours the histogram for the arrival time difference is made and a Gaussian fit is applied. In figures 17a and 17b, the means of these Gaussians are illustrated against the time. In figures 17c and 17d, the same is done for the sigmas of the fitted Gaussian.

In table 2, the means, sigmas and reduced $\chi^2$ of the fitted Gaussians are shown. The means of the Gaussians are between $-4.0 \pm 0.1$ns and $1.2 \pm 0.1$ ns, for the operational stations in the Utrecht area. The structural difference in arrival time between the two plates can be caused by several things such as the glue between the different parts of the plate is thicker for one than for the other or the lengths of the cables used for the plates are not the same. The fitted sigmas are between $5.1 \pm 0.1$ ns and $3.9 \pm 0.1$ ns. For a fit to be reasonable the reduced $\chi^2$ should be between 0.7 and 1.5. All fits are between these values and therefore can be considered as good fits.

| Station number | 1001 | 1003 | 1006 | 1007 | 1008 |
|---|---|---|---|---|---|
| Red. $\chi^2$ | 1.29 | 1.41 | 1.21 | 1.43 | 1.40 |
| Mean | -1.9 ± 0.1 | 1.2 ± 0.1 | -4.0 ± 0.1 | -0.9 ± 0.1 | 0.8 ± 0.1 |
| Sigma | 4.4 ± 0.1 | 3.9 ± 0.1 | 4.9 ± 0.1 | 4.7 ± 0.1 | 5.1 ± 0.1 |

Table 2: Reduced $\chi^2$, mean and sigma from the fitted Gaussians to the difference in arrival time for all operational stations in the Utrecht area.

### 4.4 Muon ratio

On average the same amount of particles should pass through both plates. Therefore, if we take the histogram with the distribution of the amount of muons in the plate during the event for both plates and divide those we would expect it to be one for every number of particles. However this is not the case and to verify that it is not an anamoly of one station not only station 1001 was used, but also station 1008. In figure 18, these histograms are shown. Up till ten muons in the plate the ratio is around one, after this the ratio goes down till there are 30 muons in the plate during the event; after this there are too few counts for a certain number of muons to determine a clear trend and the fluctuations get rather large.

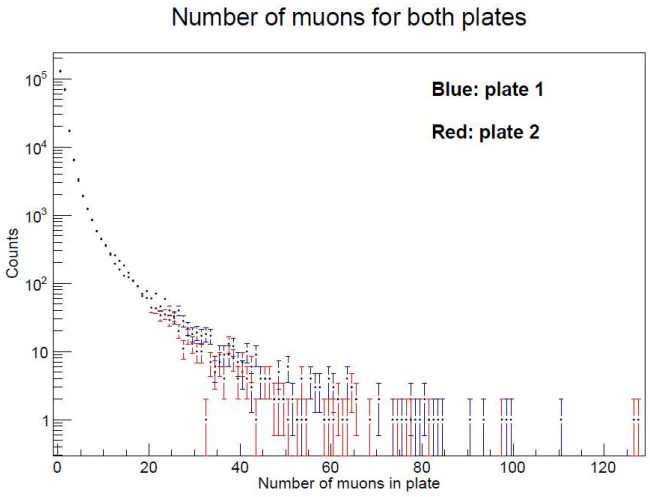


(a) Histogram of amount of muons for station 1001.

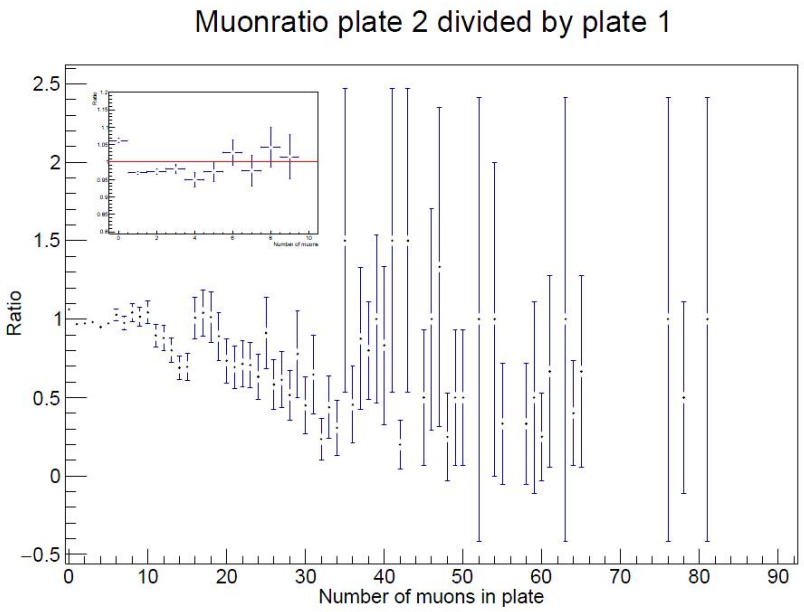


(b) Ratio of amount of muons for station 1001.

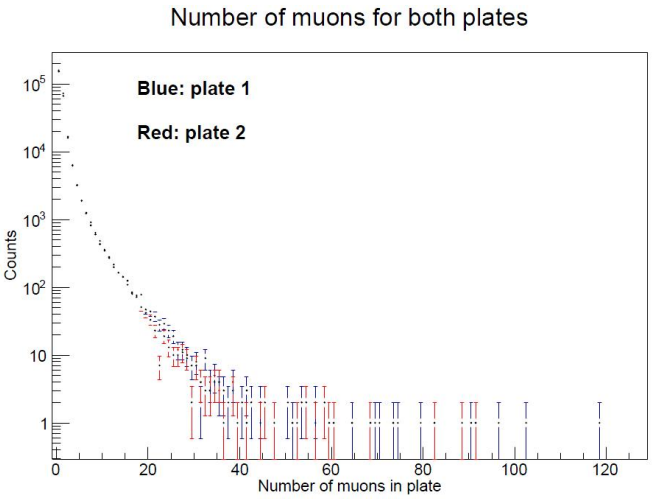


(c) Histogram of amount of muons for station 1008.

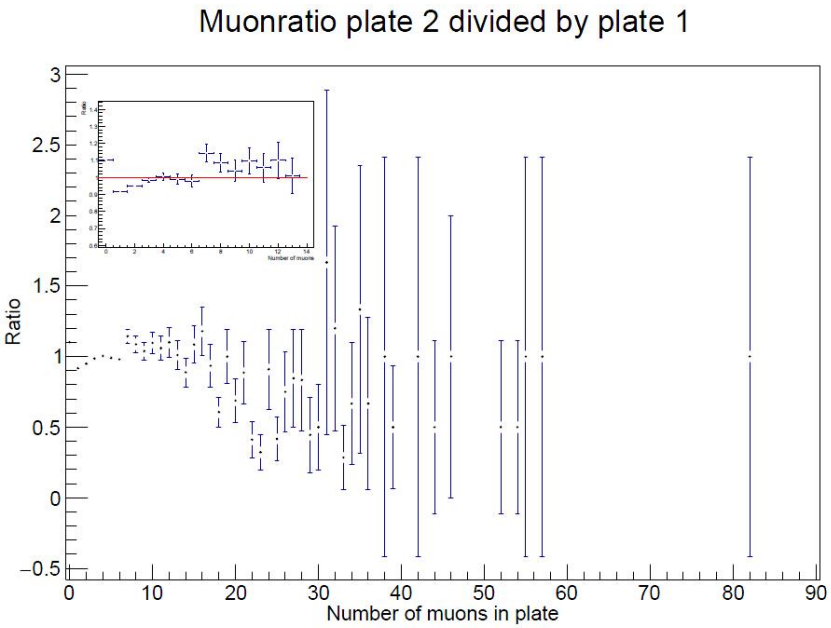


(d) Ratio of amount of muons for station 1008.

Figure 18: For stations 1001 and 1008 of the time period of a month a histogram is made of the amount of muons during an event, this is shown in figures 18a and 18c. In figures 18b and 18d, the ratio from the red and blue histograms is taken.

## 4.5 Muon distribution

One branch of the data stored of the events is the amount of muons that enter the plate during the corresponding event. This is based on the energy of the pulse. In order to check if this is done correctly we take a range of muons, for instance 2.5 till 3.5, and for this range we make a histogram of the pulseheight. This should have the shape of a Gaussian, due to the fact that we use a range, and a Landau. This is shown in figure 19.

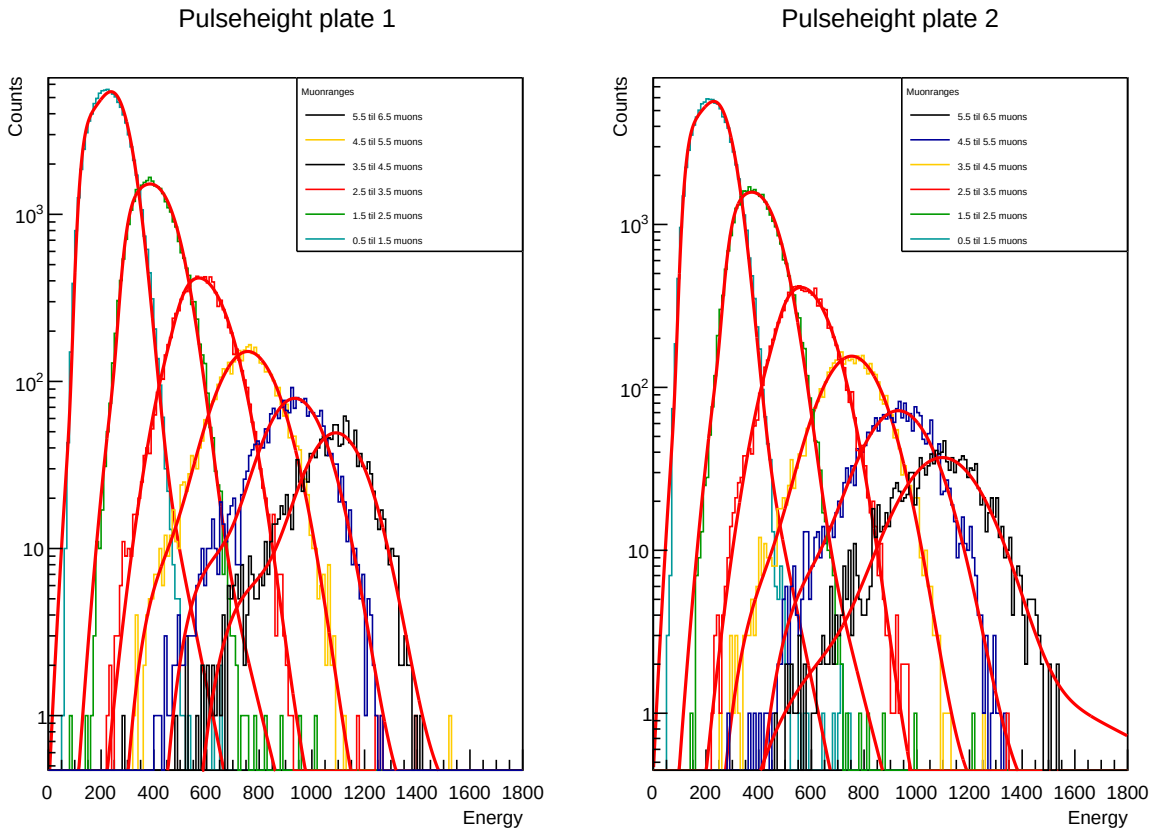


Figure 19: For station 1001 over the time period of a month for both plates of the detector histograms are made of the pulseheight in a range of amount of muons, as indicated by the legend. The red curves are the fits of a Gaussian with a Landau.

In table 3 the peaks of the Gaussian and Landau are summarised for both plates. From the figure it is evident that the peak shifts to higher energies for a bigger amount of muons in the plate. In the table, this is also visible in the position of the peak of the Gaussian and most of the Landau peaks. Only for 3.5 till 4.5 muons per event the Landau peak lowers. This could be due to the histograms from this range and higher have a larger tail towards the left than the right, whereas the ranges lower than 3.5 till 4.5 only have a tail towards the right. Also the peak of the second range, 1.5 till 2.5, is not at twice the

energy of the peak of the first range. It is slightly less than two, the same holds for the other peaks; they are at slightly less than the mean of the range times the energy value corresponding to the first peak.

| Muon range | Peak Landau plate 1 | Peak Gaussian plate1 | Peak Landau plate 2 | Peak Gaussian plate 2 |
|---|---|---|---|---|
| 0.5 till 1.5 | 156.6 ± 0.4 | 249.7 ± 0.4 | 154.7 ± 0.4 | 243.2 ± 0.4 |
| 1.5 till 2.5 | 332.4 ± 1.2 | 414.5 ± 0.8 | 328.2 ± 1.3 | 404.3 ± 0.8 |
| 2.5 till 3.5 | 543.2 ± 10.0 | 518.2 ± 1.7 | 532.7 ± 9.2 | 571.6 ± 1.7 |
| 3.5 till 4.5 | 483 ± 58 | 757.6 ± 2.7 | 495.6 ± 41.7 | 754 ± 2 |
| 4.5 till 5.5 | 654.2 ± 25.4 | 937.4 ± 3.5 | 649.8 ± 41.9 | 932.3 ± 4.1 |
| 5.5 till 6.5 | 808.8 ± 37.9 | 1094 ± 5 | 881 ± 103 | 1098 ± 6 |

Table 3: Peaks of the Gaussian and Landau fitted to the pulseheight histograms of different muon ranges for station 1001.

### 4.6 Weather conditions

In the lower 10 km that is the part that influences the weather. This could influence the amount of particles that reach the detector. In figure 20, three different weather conditions are shown over the course of a month.

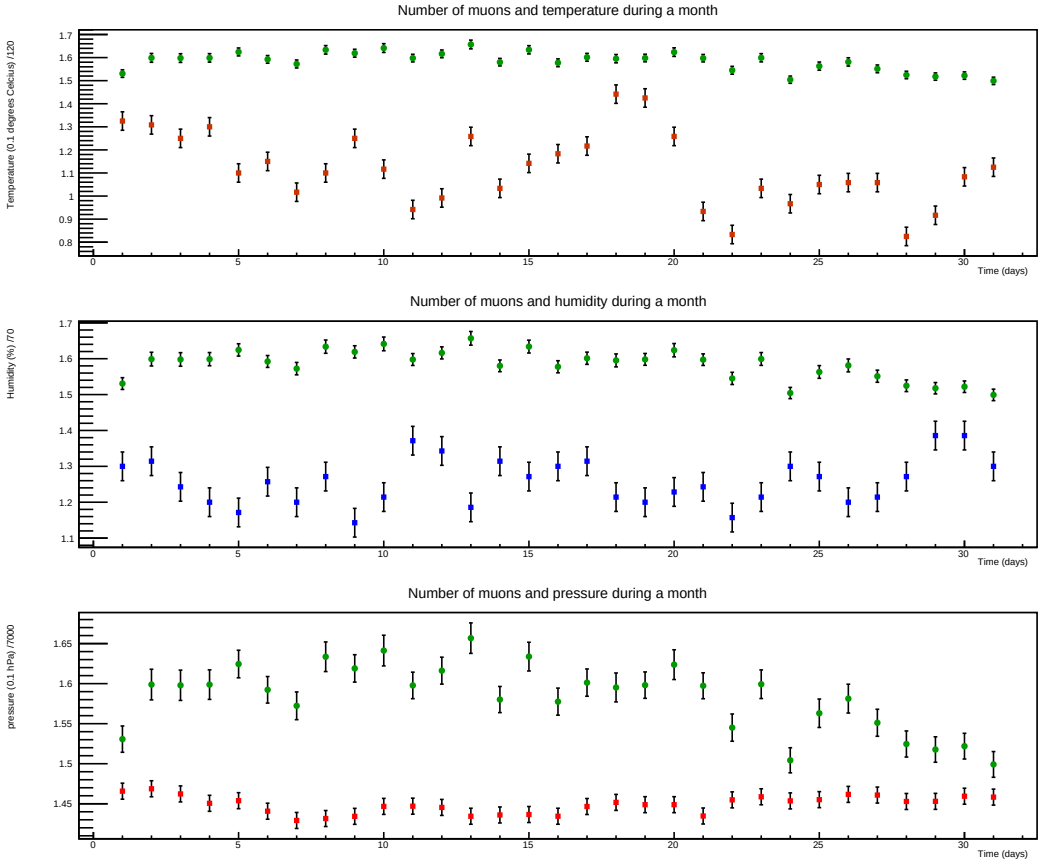


Figure 20: For a month different weather conditions, temperature, pressure and humidity, are depicted against time along with the average amount of muons per event over the same day.

For every day, the average amount of muons for an event is calculated. Then, the weather conditions are divided into intervals of all the days on which the weather condition is within a certain interval the mean of the average amount of muons is calculated. This mean is set against the mean value of the interval, resulting in a correlation between the weather condition and the average amount of muons. In figure 21, the data and the relations fitted to it are displayed. Between pressure and the amount of muons no clear correlation can be found. For temperature (T in 0.1 degrees °C) and humidity (H in %) the following relations with the average amount of muons ( $\langle\mu\rangle$ ) are found:

$$T = (1168 \pm 260) \times \langle\mu\rangle - (1713 \pm 411) \tag{2}$$

$$H = -(232 \pm 44) \times \langle\mu\rangle + (458.1 \pm 69.6) \tag{3}$$

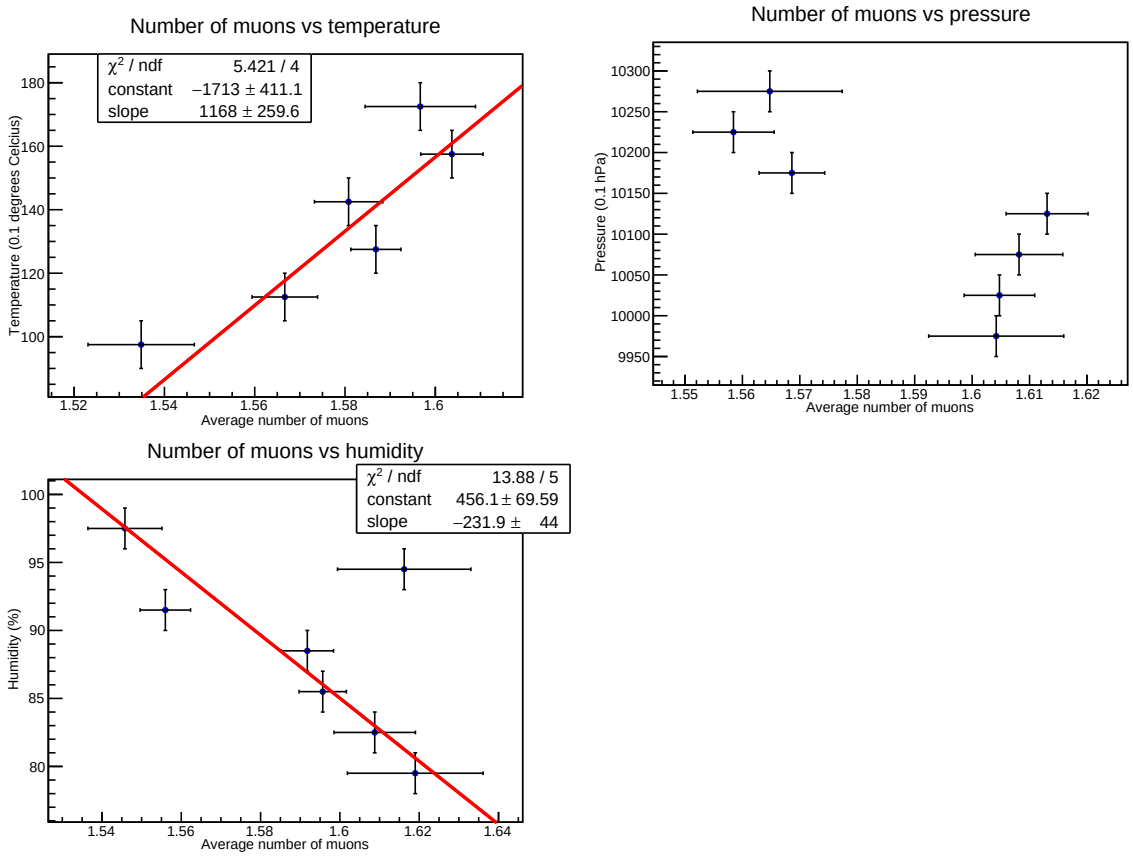


Figure 21: For intervals of the weather conditions the mean of the average amount of muons is calculated. The relations of the weather condition and the average amount of muons is fitted with a first degree polynomial.

Therefore, the average number of muons increases with increasing temperature and decreases with increasing humidity. In table 4, the percentage change of the found fits is shown. Considering that temperature has a range from at least minus five degrees up till 25 degrees Celsius temperature is the most influential factor on the average amount of muons.

| | Begin | End | Percentage |
|---|---|---|---|
| Temperature | 10.0 °C | 18.0 °C | 3.7 % increase |
| Humidity | 100 % | 80 % | 4.3 % decrease |

Table 4: Percentage difference in average amount of muons for temperature and humidity.

## 4.7 Day and night effect

During the day particles from the sun reach the detector as well as the shower particles from the cosmic rays. Therefore, we would expect the detector to detect more particles

during the day than during the night. To minimize the influence of the weather conditions several days with similar weather conditions are selected. For these days, the average amount of muons per event is calculated for every hour of the day. Then for every hour the mean of the average amount of muons is calculated. In figures 22 and 23, these means are set against hour of the day. However, the expected behaviour is not observed; there is a minimum around midday and there are two maxima at three hours before and after midnight. Even if one assumes that the particles from the sun do not cause particles that reach the detector one would expect still to see a day and night effect due to the temperature change during a day. This effect we would still expect to be a maximum during the day and a minimum during the night since we have the relation between the average amount of muons and the temperature in equation 2. Further studies are needed to understand this measurement.

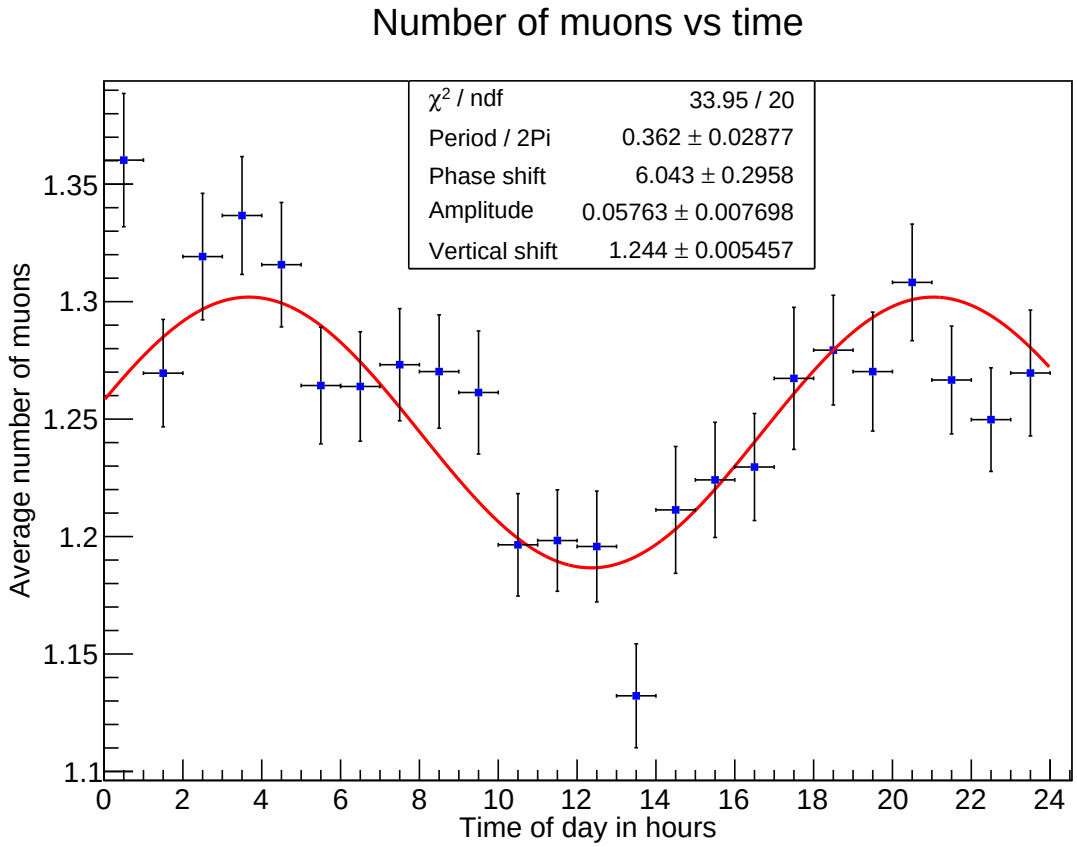


Figure 22: Mean of the average amount of muons per hour set out against time. The used days are taken in summer with similar temperature and humidity. The temperature has a range of 20.8 °C till 22.4 °C and the humidity has a range from 66% till 76%.

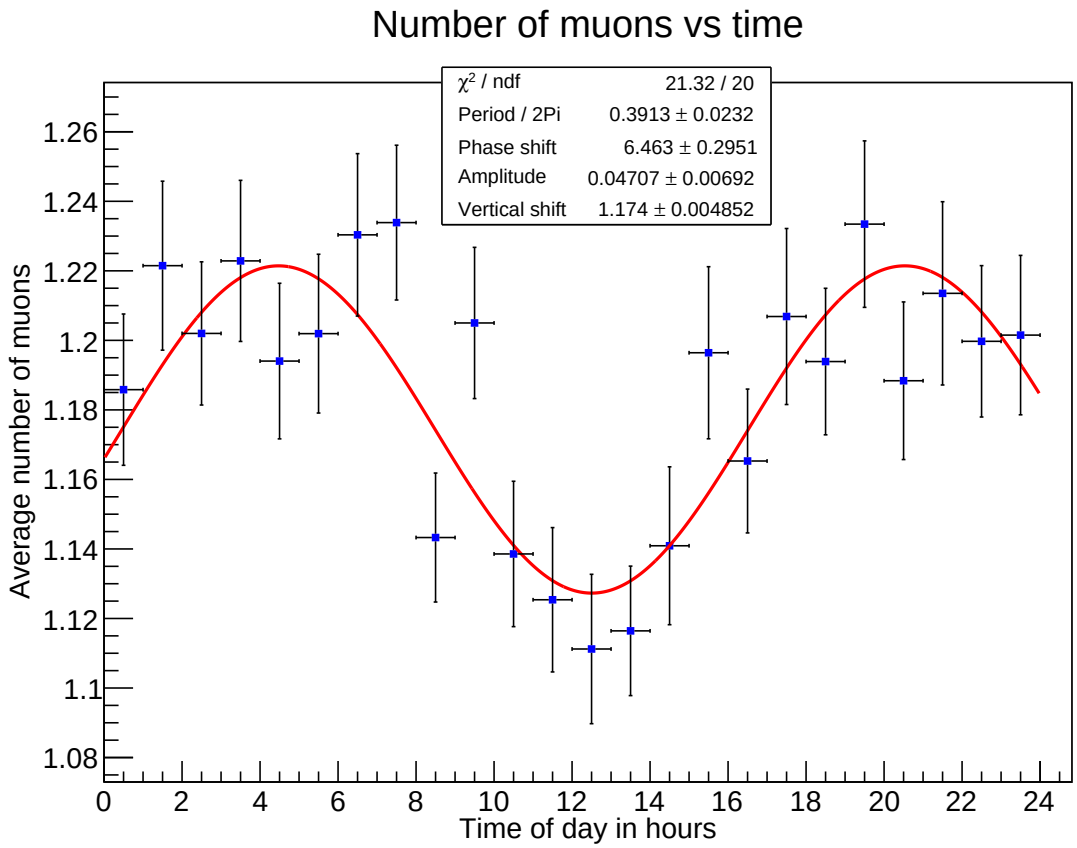


Figure 23: Mean of the average amount of muons per hour set out against time. The used days are taken in winter with similar temperature and humidity. The temperature has a range of -2.0 °C till -1.0 °C and the humidity has a range from 70 % till 80 %.

### 4.8 Seasonal effect

Due to the rotation axis of the earth being tilted, the particles that reach the detector that come from the sun will enter the atmosphere with a different inclination in summer than in winter. Due to the larger inclination in winter the particles from the sun traverse more atmosphere on winter than during summer. Therefore, on average one would expect to detect more particles in the summer than in the winter. Also the weather conditions are different in the summer, but due to the fitted correlations with the weather conditions temperature and humidity we can compensate for this and look at the true difference in average muons per event during summer and winter. In table 5, the weather conditions of the used days are shown.

| Day | Temperature | Humidity | Pressure |
|---|---|---|---|
| 2010-01-01 | -1.6 | 78 | 10026 |
| 2010-02-13 | -1.7 | 75 | 10194 |
| 2012-12-13 | -1.0 | 79 | 10089 |
| 2013-01-18 | -1.7 | 80 | 10095 |
| 2013-02-13 | -1.3 | 78 | 10244 |
| 2013-02-21 | -1.2 | 71 | 10251 |
| 2012-07-04 | 21.2 | 71 | 10124 |
| 2012-07-05 | 21.9 | 75 | 10092 |
| 2012-07-24 | 20.9 | 66 | 10185 |
| 2012-07-25 | 22.3 | 67 | 10185 |
| 2012-07-26 | 21.2 | 71 | 10178 |
| 2012-07-27 | 21.4 | 76 | 10112 |

Table 5: Weather conditions for days used in seasonal effect analysis.

In figure 24, the average number of muons per day for the days used is shown, for both the detected average amount of muons and the corrected average amount of muons. When there is no correction for the weather conditions the average amount of muons is in winter both higher and lower than in summer. However, the corrected averaged amount of muons is higher in winter than in summer. In figure 25 the ratio of the corrected version is shown. For all of the days the ratio is larger than one.

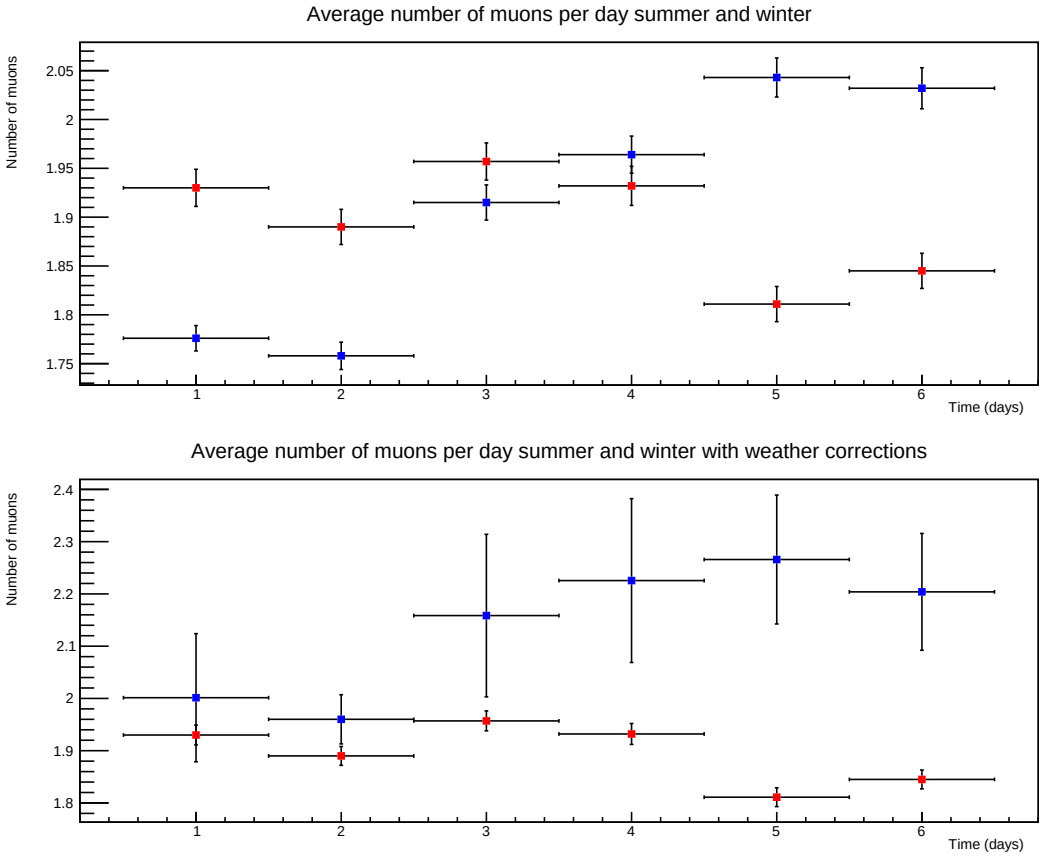


Figure 24: Average number of muons for six days in summer (red) and winter (blue). In the second graph the averaged amount of muons in winter is corrected for the weather conditions with the day it is plotted on the same day with.

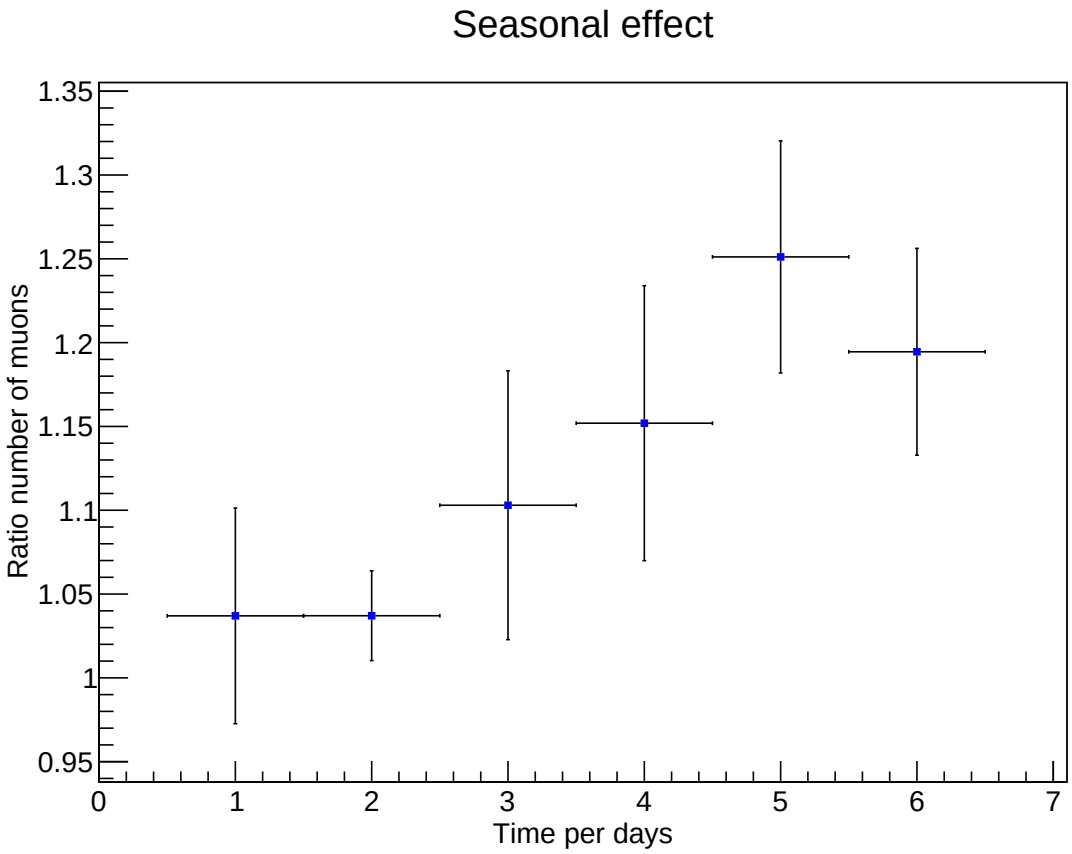


Figure 25: Ratio of the average amount of muons, winter divided by summer, where the average amount of muons is compensated for the weather conditions.

# 5 Conclusion and Outlook

With setting the pulseheight against the pulse integral one can determine the saturation point of the PMT. For the five stations in the Utrecht area is between 1800 till 2800 ADC for the pulseheight. At these values the data is no longer reliable. One could lower the voltage over the PMT to see if this influences the saturation point, however the voltage must still be in the range of the plateau of the PMT.
If the arrival time difference distribution has a Gaussian shape with a sigma of a couple nanoseconds and a mean up to a few nanoseconds as well the detector is working. For the stations in Utrecht the mean varies between $-4.0 \pm 0.1$ns and $1.2 \pm 0.1$ ns, and the sigma has a range of $5.1 \pm 0.1$ ns till $3.9 \pm 0.1$ ns. With the determined means of the Gaussians the trigger matrices could be adjusted to compensate. Also the mean and sigma of the Gaussian change less than 0.2% in two weeks and therefore they are stable in time.
Up to 30 muons in the plate per event there are enough statistics see that the ratio of the amount of muons per event of both plates is stable up till about ten muons and after this there is a downward trend. There is no clear explanation for this downward trend and additional research is needed to determine if the events that are listed as more than ten mouns during the event provides accurate and thereby usable data.
The peak of the pulseheight distribution for increasing ranges of muons shifts to right as expected. However, the peak of an average of two muons in the plate does not correspond with twice the energy of one muon in the plate. Also, there is a drop in the position of the peak of the Landau; this could be due to the tail change.
The weather conditions have a clear linear dependence of the average amount of muons ( $\langle\mu\rangle$ ) with temperature (T in 0.1 degrees °C): $T = (1168 \pm 260) \times \langle\mu\rangle - (1713 \pm 411)$. Humidity (H in %) has the opposite behaviour: $H = -(232 \pm 44) \times \langle\mu\rangle + (458.1 \pm 69.6)$. When the humidity is higher there are more water molecules in the air, thereby the shower particles will have a higher chance of interaction. In order to determine if the average amount of muons is truly uncorrelated with the pressure the analysis must be done over a longer period of time than a month.
The opposite behaviour than expected is found for the day and night effect. Also, the period of the sine function is not one day, but about $\frac{2}{3}$ of a day. In another research, the expected behaviour with a maximum during the day and a minimum at midnight and a time period of a day was found [29]. The daily temperature cycle would in theory still demand the maximum during the day and a minimum during the night. Additional research is needed to study why this result occurs and if the expected behaviour can be measured with the HiSPARC detectors. From the seasonal effect analysis one could conclude that the average amount of muons is higher in winter than it is in summer. In this research, the days used are not from the same year, so one could do the same for days in winter and summer of the same year and over a longer period of time.

# References


[1] Troisième mémoire sur l'Electricité et le Magnétisme, C. A. de Coulomb, Histoire de lAcadmie Royale des Sciences, 612638 (1785)

[2] A penetrating radiation from the Earths surface, E. Rutherford & H. L. Cooke, Minutes of the Eighteenth Meeting of the American Physical Society. Phys. Rev.16, 183 (1903)

[3] Some experiments on the electrical conductivity of atmospheric air, J. C. McLennan & F. Burton, Minutes of the Eighteenth Meeting of the American Physical Society. Phys. Rev. 16, 184192 (1903)

[4] The radioactive materials of the earth and air as the origin of the invasive radiation in the atmosphere, K. Kurz, Phys. Zeit. 10, 834845 (1909)

[5] Observations in low level radiation during seven free balloon flights, V. F. Hess, Phys. Zeit. 13, 10841091 (1912)

[6] The origins of penetrating radiation, V. F. Hess, Phys. Zeit 14, 6120617 (1913)

[7] High frequency rays of cosmic origin III. Measurements in snow-fed lakes at high altitudes, R. A. Millikan & G. H. Cameron, Phys. Rev. 28, 851868 (1926)

[8] Compton, A. H. A geographic study of cosmic-rays, Phys. Rev. 43, 387403 (1933)

[9] The Hisparc Experiment: data acquisition and reconstruction of shower direction, D. B. R. A. Fokkema, ISBN: 9789036534383 (2012)

[10] Elemental Composition and Energy Spectra of Galactic Cosmic Rays During Solar Cycle 23, J. George, K. Lave, M. Wiedenbeck, et al., Astroph. J. 698, 1666 1681 (2009)

[11] Astronomy and Astrophysics Numerical Data and Functional Relationships in Science and Technology Volume 4B: Solar System, K. Lodders, H. Palme & H. P. Gail, ISBN:9783540880547, Springer (2009)

[12] Measurement of Cosmic-Ray Hydrogen and Helium and Their Isotopic Composition with the BESS Experiment, J. Z. Wang, E. S. Seo, et al., The Astrophysical Journal 564, 244 (2002)

[13] Observations of the Li, Be, and B isotopes and constraints on cosmic-ray propagation, G. De Nolfo, I. Moskalenko, et al., Advances in Space Research 38, 15581564. ISSN: 0273-1177 (2006)

[14] Astroparticle physics, C. Grupen, ISBN: 9783540253129, Springer (2005)

[15] Search for Cosmic-Ray Antimatter, G. F. Smoot, A. Buffington & C. D. Orth, Phys. Rev. Lett. 35, 258261 (1975)

[16] Antimatter research in space, P. Picozza & A. Morselli, Journal of Physics G: Nuclear and Particle Physics 29, 903 (2003).

[17] New Estimation of the Spectral Index of High-Energy Cosmic Rays as Determined by the Compton-Getting Anisotropy, M. Amenomori, et al., The Astrophysical Journal Letters 672, L53 (2008)

[18] Models of the knee in the energy spectrum of cosmic rays, J. R. Hrandel, Astroparticle Physics 21, 241265. ISSN: 0927-6505 (2004)

[19] Evidence for correlated changes in the spectrum and composition of cosmic rays at extremely high energies, D. J. Bird, et al., Phys. Rev. Lett. 71, 34013404 (1993)

[20] Cosmic rays at the energy frontier, J. Cronin, S. Swordy & T. Gaisser, Sci.Am. 76, 3237 (1997)

[21] On the Origin of the Cosmic Radiation, E. Fermi, Rev. 75, 1169 (1949)

[22] An extended Heitler-Matthews model for the full hadronic cascade in cosmic air showers, J. M. C. Montanus, NIKHEF (2014)

[23] The Quantum Theory of Radiation, W. Heitler, ISBN: 9780486645582, Dover publications (1954)

[24] High Energy Cosmic Rays, T. Stanev, ISBN: 3 540 40653 0, Springer-Praxis (2004)

[25] www.hisparc.nl/over-hisparc/hisparc-detector

[26] Detector bouw, A. P. L. S. de Laat & J. G. Oldenziel

[27] data.hisparc.nl/data/download

[28] data.hisparc.nl/show/stations_on_map

[29] Correlations between solar events and the cosmic muon flux measured with WILLI detector, I. M. Brancus, et al., procceedings of $31^{\text{th}}$ ICRC (2009)